Studies on scalability and scaling laws for the plasma focus: similarities and differences in devices from 1 MJ to 0.1 J

2010 Plasma Sources Sci. Technol. 19 055017

(http://iopscience.iop.org/0963-0252/19/5/055017)

Plasma Sources Sci. Technol. **19** (2010) 055017 (9pp) doi:10.1088/0963-0252/19/5/055017

Studies on scalability and scaling laws for the plasma focus: similarities and differences in devices from 1 MJ to 0.1 J*

Leopoldo Soto[1,2,4], **Cristian Pavez**[1,2], **Ariel Tarifeño**[2,3], **José Moreno**[1,2] and **Felipe Veloso**[1,2]

[1] Comisión Chilena de Energía Nuclear, Casilla 188-D, Santiago, Chile
[2] Center for Research and Applications in Plasma Physics and Pulsed Power, P[4], Santiago-Curicó, Chile
[3] Universidad de Concepción, Barrio Universitario, Concepción, Chile

E-mail: lsoto@cchen.cl

Received 16 August 2009, in final form 14 May 2010
Published 20 September 2010
Online at stacks.iop.org/PSST/19/055017

Abstract
A comprehensive analysis of scaling laws for plasma focus devices producing neutrons is presented. Similarities and differences in plasma focus devices working with stored energies ranging from 1 MJ to 0.1 J are found. First, a brief review listing the most important results achieved by the Thermonuclear Plasma Department of the Chilean Nuclear Energy Commission, CCHEN, is presented. The aim of the work at CCHEN has been to characterize the physics of dense plasma foci and also to carry out the design and construction of smaller devices—in terms of both input energy and size—capable of providing dense hot plasmas. Certain scaling rules have been found from this research. These rules combined with other scaling laws have been applied to design and construct plasma focus devices with storage energy in a region never explored before (tens of joules and less than 1 J). Thus, a comprehensive analysis also including results from other groups is presented. In particular, all the devices, from the largest to the smallest, maintain the same value of ion density, magnetic field, plasma sheath velocity, Alfvén speed and the quantity of energy per particle. Therefore, fusion reactions are even possible to obtain in ultraminiature devices (driven by generators of 0.1 J for example), as they are in the larger devices (driven by generators of 1 MJ). However, the stability of the plasma pinch highly depends on the size and energy of the device.

1. Introduction

Originally, in the last century (1960s, 1970s and 1980s inclusive), the plasma focus (PF) was studied as a possible device for controlled thermonuclear fusion. However, the main mechanisms producing neutrons are the thermonuclear and the beam target, the beam target being the dominant mechanism. At present, on the one hand, there are some suggestions to increase the thermonuclear component of neutron production over the beam target component in the hope of obtaining a device relevant to thermonuclear fusion studies [1, 2]. On the other hand, as the PF is an intense pulsed non-radioactive source of radiation (x-rays, XUV and neutrons), there is a renewed interest in the development of transportable and portable plasma foci for industrial and field applications, as nanoflashes of radiation. A new generation of very small, fast and compact devices has been developed during the present century [2–12].

A PF is a kind of pinch discharge in which a high-pulsed voltage is applied to a low-pressure gas between coaxial cylindrical electrodes, generating a short-duration high-density plasma region in the axis (pinch) [2]. The maximum pinch compression should be close to the peak current in order to achieve the best efficiency. Two geometries were proposed for these devices differing in their electrodes' aspect ratio (electrode length divided by inner electrode diameter): the Filipov configuration [13], with an aspect ratio <1 (typical values are 0.2) and the Mather configuration [14],

* This paper was presented as an invited talk at the 29th International Conference on Phenomena in Ionized Gases (ICPIG XXIX) held in Cancun, Mexico on 12–17 July 2009. See stacks.iop.org/PSST/19/3

[4] Author to whom any correspondence should be addressed.

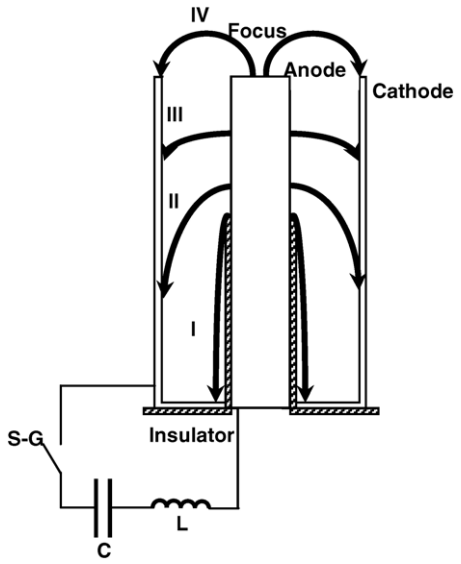

Figure 1. A scheme of the equivalent circuit and the plasma dynamics are shown. The capacitor C is discharged over the electrode through a spark gap (SG). The plasma dynamics is sketched in a side section of the electrodes, I: the discharge starts over the insulator, II, III: the current sheath is accelerated along the coaxial electrodes and IV: pinch.

with an aspect ratio >1 (typically 5–10). Also, devices with a hybrid aspect ratio (typically 1 to 2) have been developed [2–9, 15, 16].

Figure 1 shows the scheme of the equivalent electrical circuit and the discharge evolution in a Mather type PF. The electrodes are in the vertical position; the anode at the center is partially covered from its base by a coaxial insulator. The discharge starts over the insulator surface. Then, the plasma sheath comes off and it is axially accelerated by the magnetic field self-generated by the current. After the current sheath runs over the upper end of the central electrode, the plasma is compressed in a small region (the focus or pinch). In most of the devices, these three stages last a few microseconds, and less than 500 ns in the new generation of fast plasma foci [2]. The maximum pinch compression should be close to the peak current in order to achieve the best efficiency. Depending on the energy of the pulse power generator, the current in the pinch varies from tens of kiloamperes to some mega-amperes. The pinch generates beams of ions and electrons, and ultrashort x-ray pulses. The duration of these pulses is of the order of a few nanoseconds to hundreds of nanoseconds. Using deuterium gas, PF devices produce fusion D–D reactions, generating fast-neutron pulses (∼2.5 MeV) and protons (leaving behind ^{3}He and ^{3}H).

Scaling laws for neutron yield and the scalability properties in PF devices have been a subject of study since early PF research [45, 46]. From experimental data compiled during the past decades, scaling laws for neutron yield, Y, were established in the 1970s and 1980s. From different optimized devices that operate with D_2 in a particular stored energy from a few kilojoules to hundreds of kilojoules, most authors agree that Y scale as $Y \sim E^2$ and $Y \sim I_0^{3.3}$ (where E is the initial stored energy in the capacitor bank and I_0 the pinch current [47]. On the other hand, using the data of 117 experiments it has been found that Y goes as $Y \sim I_0^{4.0–4.7}$ [10, 42]. Recent works based on numerical experiments [48–50] have shown that the yield scales as $Y \sim E^2$ and $Y \sim I_0^{4.5}$ for low kilojoules and sub-kilojoules devices, while for high kilojoules and megajoules PF devices the scaling is deteriorating for energy as $Y \sim E^{0.8}$, but scaling with the current is maintained as $Y \sim I_0^{4.5}$. In addition, it is well known that the axial and radial velocities of the plasma sheath are proportional to $(I_o/ap^{1/2})$ (where a is the anode radius, and p is the gas filling pressure or mass density filling pressure) [29]. Lee and Serban [17] observed in the 1990s that $(I_o/ap^{1/2})$, called 'drive parameter' by them, has an average value of 77 kA cm^{-1} mbar$^{-1/2}$ with a small variation of 10% for PF devices experimentally optimized for neutron production. A few years ago, Soto [2, 7] extended this observation to PF devices working with stored energy of hundreds and tens of joules. Soto also introduced the 'energy density parameter' $(28E/a^3)$ as an additional observation to the PF common parameters. The value for the energy density parameter is (1–10) × 10^{10} J m^{-3} for devices working from 1 MJ to 50 J. At present, the constancy of the drive parameter and that of the energy density parameter are useful design tools for PF devices.

2. Research program at the Chilean Nuclear Energy Commission

In the last few years, on the one hand, a few works on PF configuration using the SPEED2 generator charging at 70 kJ have been made at the Chilean Nuclear Energy Commission (CCHEN). On the other hand, experimental studies in PF have been extended to devices operating under 1 kJ, in the range of hundreds and tens of joules [3–8]. Moreover, a device that operates with only 100 mJ has recently been designed and constructed at CCHEN [9]. The experiments at CCHEN have been performed in the following devices: SPEED2 (70 kJ), PF-400J (400 J), PF-50J (50 and 67 J) and Nanofocus, NF (0.1 and 0.26 J). Further details of these experiments and their diagnostics can be found elsewhere [3–9, 18, 19]. The research work includes the study of neutron yield, angular distribution of neutrons, energy distribution of neutrons, x-ray emission, plasma dynamics and density measurements.

The results obtained in the PF research program at CCHEN can be summarized as follows.

Neutron yield. Neutron yield versus deuterium filled pressure has been obtained for PF-400J operating at ∼400 J and for PF-50J operating at 50 and 70 J. The maximum measured neutron yield was (1.06 ± 0.13) × 10^6 neutrons per shot at 9 mbar in the PF-400J [6] and (3.6±1.5) × 10^4 neutrons per shot at 9 mbar in the PF-50J operating at 67 J and (1.3 ± 0.5) × 10^4 neutrons per shot at 6 mbar in the PF-50J operating at 50 J [8]. From these results, the following scaling laws for PF devices operating under 1 kJ have been obtained: $Y \sim 7.73 \times 10^{-5} I_o^{4.82}$ (with I_o the pinch current in kA), $Y \sim 3.15E^{2.13}$ (with E the energy in the capacitor bank in J). If additional data obtained recently by other groups are considered [10–12], similar power dependences are obtained for sub-kilojoules

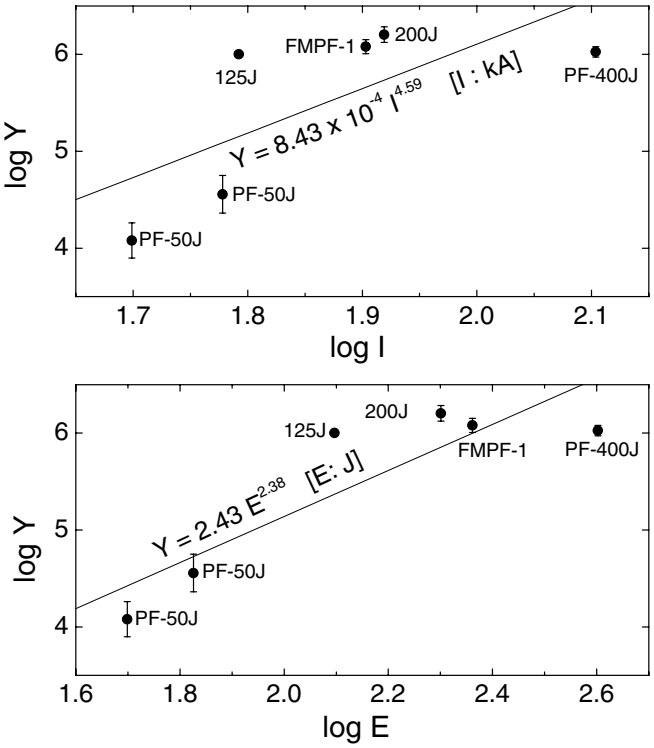

Figure 2. Neutron yield, Y, scaling laws for sub-kilojoules PF devices (I: current, E: stored energy). Data include results from CCHEN (PF-400J [6], PF-50J [8]) and others groups (125 J [10], 200 J [11], FMPF-1 [12]).

PF devices: $Y \sim 8.43 \times 10^{-4} I_o^{4.59}$, $Y \sim 2.43 E^{2.38}$ (as shown in figure 2). This result is consistent with scaling laws with numerical experiments for a few kilojoules and sub-kilojoules devices [48, 50].

In the SPEED2 the neutron yield versus deuterium filled pressure is still being characterized. SPEED2 uses a special insulator, quartz covered with alumina, and it requires several shots of preparation in order to obtain a neutron yield with dispersion lower than 30% between shots. We have not had enough shots with the same insulator in order to achieve the proper conditions of operation. Preliminary results obtained at CCHEN show a neutron yield of the order of 10^{10} neutrons per shot; the maximum value obtained till now at CCHEN is 2×10^{10} neutrons per shot at 2–3 mbar, 70 kJ, 2.4 MA. In Düsseldorf, a neutron yield of the order of 10^{11}–10^{12} neutrons per shot was obtained [20].

A repetitive PF, PFR, which works at 30 kV with deuterium at a pressure of 9.2 mbar with a repetition rate from 3 to 6 Hz was developed. It produces $(2.1 \pm 0.34) \times 10^7$ neutrons, for each burst of 5 s duration, i.e. 15 to 30 shots per burst.

In addition, evidence of neutron emission has been observed in the ultraminiature device Nanofocus operating at 0.1 J of stored energy and 20 Hz of repetition rate. However, the reproducibility of this miniature device is low and several technological subjects have to be previously solved in order to produce neutrons for periods greater than minutes. Due to the low reproducibility of the Nanofocus and the fact that the device has not yet been optimized, the data of its neutron yield were not included in the plot of figure 2.

Angular distribution of neutron emission. Angular distribution of neutron emission was obtained in the PF-400J device using CR-39 nuclear track detectors covered with polyethylene located at several positions (between -90° to 90°). The angular measurements were compared with the total neutron yield (integral of the angular measurements). The results are consistent with an angular uniform plateau (isotropic emission) plus a shape peaked in the direction of the axis of the discharge (anisotropic emission). Isotropic components account for 57.5% of the accumulative emission, while the anisotropy component accounts for the remaining 42.5%. The anisotropic component appears between $+50^\circ$ and -50° approximately [21].

Energy distribution of the neutrons. Five scintillation detectors (scintillator + photomultiplier) were located at different distances in radial orientation with the discharge in the PF-400J; the energy spectrum was obtained [21], with an average energy and dispersion of (2.5 ± 1) MeV. In the case of the PF-50J only two scintillation detectors were used and the energy of the neutrons was estimated to be 2.7 ± 1.8 MeV [8].

X-ray emission. Hard x-ray emission has been studied in the PF-400J using a commercial radiographic recording system (13×18 cm^2), Curix ST-G2 from AGFA was used together with AGFA suggested developer and fixer for this film. The film is placed inside a plastic light tight cassette, Curix from AGFA, containing intensifying plastic screen sensitive to x-radiation. The cassette with the film was placed as close to the object to be imaged as possible to improve the image quality. The object is placed between the PF device and the cassette. A photomultiplier tube with a plastic scintillator is used to monitor the x-ray emission in each shot. This diagnostic is placed perpendicularly to the symmetry axis at the anode top level. Radiographs of an array of filters of different materials of millimeter thickness were obtained with the PF-400J.

In order to estimate the average energy of the x-ray emitted by the PF devices, a monoenergetic radiation was assumed. When a monoenergetic radiation interacts with an element, the classical exponential radiation decay relation through the matter is $I(x)/I_0 = \exp(-K \cdot x)$, where $I(x)/I_0$ is the normalized radiation intensity after traveling a distance x inside the material characterized by a linear attenuation coefficient K. From this relation, it is possible to obtain the effective linear attenuation coefficient K when different gray shades of the digitalized images are linked to the $I(x)/I_0$ ratio. This method provides a correlation between K and the x-ray energy [22]. Thus, an effective mean energy of 90 ± 5 keV was obtained for the PF-400J using the Curix ST-G2 AGFA system as the recording media.

The same method was used to characterize the x-ray emission from the Nanofocus device operating at 0.1 J. Radiographs of an array of aluminum filters of 30, 45 and 60 μm on a HP5 Ilford film were obtained by integrating 1200 shots on the film. In this case, an effective mean energy of 4.3 ± 0.3 keV was obtained [23].

Plasma dynamics and electron density. An intensified CCD camera (ICCD) gated at 5 ns exposure time and synchronized with the discharge has been used in order to obtain the side view images of the visible light emitted from the plasma. A sequence of the plasma dynamics was obtained for the PF-50J [5]. From the observations, an average radial velocity of the order of $10^5\,\mathrm{m\,s^{-1}}$ was obtained. It was also found that the plasma velocity speeds up nearly twice its value close to the pinching time. The final pinch radius observed was of the order of $0.12a$, with a the anode radius. This diagnostic was also used to characterize the plasma motion in the Nanofocus device. The dynamics observed from the photographs in this ultraminiaturized device operating at only 0.1 J is consistent with the dynamics observed in devices operating at energies several orders of magnitude higher: (a) formation of a plasma sheath close to the insulator surface, (b) the plasma covering the anode, (c) radial compression over the anode and (d) finally the plasma is detached from the anode in the axial direction [9].

In addition, a refractive optical system was employed in order to measure the electron density and the dimensions of the pinch column. A Mach–Zehnder interferometer using a pulsed Nd-YAG laser was employed (600 mJ, 532 nm, 8 ns) [19, 24]. The diagnostic was applied to the PF-400J and PF-50J devices. A maximum electron density of $(8.4 \pm 1.3) \times 10^{24}\,\mathrm{m^{-3}}$ was measured on the axis in the PF-400J operated in H_2 [24] and of $(1.5 \pm 0.2) \times 10^{25}\,\mathrm{m^{-3}}$ in the PF-50J operated in D_2 [19]. The pinch radius observed with this method in the PF-400J was of the order of $0.12a$, and between $0.1a$ and $0.2a$ in the PF-50J. The corresponding line density was measured in $(8.6 \pm 1) \times 10^{18}\,\mathrm{m^{-1}}$ for the PF-400J operated in H_2 and in $(2.2 \pm 0.3) \times 10^{18}\,\mathrm{m^{-1}}$ for the PF-50J operated in D_2. In addition, in the PF-50J, a temporal sequence of interferograms was obtained and the same radial velocities obtained with the ICCD camera were measured (of the order of $10^5\,\mathrm{m\,s^{-1}}$ for the average radial velocity and $\sim 2 \times 10^5\,\mathrm{m\,s^{-1}}$ close to the pinch moment) [19].

Table 1 summarizes the main characteristics of the PF devices at the CCHEN.

Even though the results obtained in our laboratory devoted to x-ray emission have been summarized and some papers related to the study of scaling laws for x-rays or particle emission in PF devices are available [43, 44], there is insufficient information to propose a comprehensive analysis related to scaling laws of x-rays and other emission for PF devices. In the next section a discussion on scalability properties, scaling laws, similarities and differences among PF devices optimized for neutron emission is presented.

3. Discussion

A common feature of PF devices is the existence of plasma parameters that remain relatively constant for facilities in every optimized plasma foci for neutron production in a wide range of energy, from a few kilojoules to 1 MJ: electron density $\sim 10^{25}\,\mathrm{m^{-3}}$, temperature in the range 300 eV–1 keV, and the velocity of the current sheath with an average value of $\sim 1 \times 10^5\,\mathrm{m\,s^{-1}}$ in the axial phase and $\sim 2.5 \times 105\,\mathrm{m\,s^{-1}}$ at the end of the pinch compression. At the CCHEN, these observations have been extended to devices working with stored energy under 1 kJ, to hundreds and tens of joules (section 2 and table 1). It is interesting to point out that the plasma parameters (which remain practically constant in PF devices) are correlated with the value of electrical and geometrical parameters of the devices through to the drive parameter $I_o/ap^{1/2}$ and the energy density parameter $28E/a^3$. Table 2 shows the value of these parameters for devices with stored energies ranging from 1 MJ to 0.1 J. More devices in the range of hundreds of joules reported recently are included, complementing the data tabulated previously in [2, 7, 17].

From table 2, if only the data for optimized PF devices emitting neutrons are considered it is clear that when the initial stored energy varies by a factor of 10^8, the drive parameter varies only by a factor of 2, the energy density parameter varies by a factor of ~ 10 and the energy per mass parameter varies by a factor of 23.

3.1. Similarities

A discussion about the significance of the drive parameter and of the energy density parameter allows one to understand the similarities observed in PF devices ranging eight orders of magnitude in energy.

The drive parameter and its importance in the performance of PF as a source of fusion neutrons were discussed by Lee and Serban [17]. Simple models to describe the PF dynamics show that $I/ap^{1/2}$ is relevant. The model developed by Lee describes the axial phase of the dynamics by a snow-plow model and the radial phase by a slug model [4, 30]. The coupling of drive magnetic field to the plasma sheath in the axial and radial phases, using either the snow-plow or the slug model, indicates that the characteristic axial velocity, v_a, and radial velocity, v_r, both depend on $I/ap^{1/2}$. Thus,

$$v_a \propto I/ap^{1/2},$$

$$v_r \propto I/ap^{1/2}.$$

Note that the magnetic pressure, $B^2/2\mu \propto (I/a)^2$, is the magnetic energy per unit volume associated with the current I flowing in radius a. Dividing by the mass density ρ (or p, given that $\rho \propto p$), the magnetic energy per unit mass is obtained. Thus, magnetic energy per unit mass $\propto (I/a)^2/p \equiv \zeta^2$.

Zhang *et al* [31] note a simple consistent picture. The magnetic piston delivering magnetic energy per unit mass $\propto \zeta^2$ drives the shock system to velocity ζ with kinetic energy per unit mass $\propto \zeta^2$.

The energy density parameter was introduced by Soto [2, 7] as a way to compare different PF devices. Although only a fraction of the initial energy E stored in the capacitor bank is transferred to the plasma, the parameter E/V_p (where V_p is the final pinch volume) is often used to characterize the plasma energy density in order to compare different devices. According to scaling numerical simulations [17, 30] and experimental observations [5, 8, 17, 19] the final pinch radius r_p (prior to the appearance of instabilities with the subsequent appearance of smaller inhomogeneities in the plasma column) is of the order of $0.12a$ and the maximum pinch height is of the order $0.8a$. Thus the final plasma volume V_p (prior to the appearance of probable instabilities)

Table 1. Main characteristics of the PF devices at CCHEN and experimental observations.

	Device				
	SPEED2 [41]	SPEED4	PF-400J [6]	PF-50J [8, 19]	NF [9]
Capacity (nF)	4.16[a]	1.25[a]	880	160	5
Charging voltage (kV)					
Maximum	300	100	35	35	15
Typical operation	150	60	30	25–30	5–10
Inductance (nH)	20	40	38	38	5
Time to peak current (ns)	400	350	300	150	16
Stored energy (J)					
Maximum	187	6.25	540	100	0.56
Typical operation	67	2.25	400	50–70	0.1
Peak current (kA)					
Maximum	4000	550	168	70	15
Typical operation	2400	330	127	50–60	5–10
Anode					
Radius (cm)	5.4	1.6	0.6	0.3	0.08–0.022
Material	Copper	Copper	Copper	Copper	Copper
Cathode					
Radius (cm)	11	4.5	1.3	1.1	—
Material	Copper	Copper	Copper	Copper	Copper
Effective anode length (cm)	1.5–2.5	1–2	0.7	0.48	0.04
Insulator					
Length (cm)	6.5	2.7–3.9	2.1	2.4	1
Material	Quartz covered with alumina	Alumina	Alumina	Alumina	Quartz and alumina
Size (capacitor bank and discharge chamber)	8 m × 8 m × 2 m	1 m × 1 m × 0.5 m	50 cm × 30 cm × 30 cm	50 cm × 30 cm × 20 cm	25 cm × 25 cm × 5 cm
Weight (capacitor bank and discharge chamber) (kg)	10 000	200	50	50	5
Maximum repetition rate (Hz)			1	1	50
Typical operation (Hz)	Single shot	Single shot	Single shot	Single shot	1–20
Neutron yield per shot	$\sim 10^{11}$–10^{12} (Düsseldorf) [20] $\sim 2 \times 10^{10}$ (CCHEN)	—	1.2×10^6 at 400 J and 9 mbar in D_2	3.6×10^4 at 70 J and 9 mbar in D_2 1.3×10^4 at 50 J and 6 mbar in D_2	10^2 with low reproducibility
Ion density on the axis n (m^{-3})	—	—	$(8.4 \pm 1.3) \times 10^{24}$ in H_2	$(1.5 \pm 0.2) \times 10^{25}$ in D_2	—
Number of ions per unit length (line density) N (m^{-1})	—	—	$(8.6 \pm 1) \times 10^{18}$ in H_2	$(2.2 \pm 0.3) \times 10^{18}$ in D_2	—
Energy of the neutrons ± dispersion (MeV)	—	—	2.5 ± 1	2.7 ± 1.8	—
Maximum neutron flux in repetitive operation	—	—	10^6 n s^{-1}	3.6×10^4 n s^{-1}	$\sim 10^3$–10^4 n s^{-1} expected for short periods (less than 1 min.)

[a] Equivalent capacity of the SPEED generators.

Table 2. The drive parameter ($I_o/ap^{1/2}$) and the density energy parameter ($28E/a^3$) are listed for various PF devices, E is the stored energy in the capacitor bank, I_o is the peak current, a the anode radius and p the gas filling pressure for the maximum neutron yield.

Device [reference]-location	Energy E (kJ)	Anode radius a (cm)	Peak current (kA)	Pressure (mbar)	Energy density parameter $28\ E/a^3$ (J m^{-3})	Drive parameter $I/p^{1/2}a$ (kA mbar$^{-1/2}$ cm^{-1})	Energy per mass parameter E/a^3p ($\times 10^7$ J m^{-3} mbar^{-1})
PF-1000 [25]-Poland	1064	12.2	2300	6.6	1.6×10^{10}	73.4	8.5
PF-360 [26]-Poland	130	6	1200	1.6	1.7×10^{10}	61.4	38
SPEED2 [2]-Chile	70	5.4	2400	2.7	1.2×10^{10}	—	15.9
7 kJ PF [27]-Japan	7	1.75	390	6	3.7×10^{10}	91	22
GN1 [28]-Argentina	4.7	1.9	—	—	1.9×10^{10}	—	—
Fuego Nuevo II [16] Mexico	4.6	2.5	350	3.7	0.8×10^{10}	73	7.7
UNU/ICTP-PF [29]-Asia and Africa	2.9	0.95	172	8.5	9.5×10^{10}	81	4.1
PACO[a] [15, 16]-Argentina	2	2.5	250	1.5	3.6×10^{9}	95	8.5
PF-400J [6]-Chile	0.4	0.6	127	9	5.2×10^{10}	70	2
FMPF-1 [12] Singapore	0.23	0.35	80	5.5	1.5×10^{11}	97	5.35
200J[a] Batt-PF [11] India	0.2	0.5	83	10	4.5×10^{10}	52[a]	1.6[a]
125J PF [10] Argentina	0.125	0.75	62	2	0.83×10^{10}	58[a]	1.5[a]
PF-50J [2, 8]-Chile	0.07	0.3	60	9	7.3×10^{10}	66.7	2.9
	0.05	0.3	50	6	5.2×10^{10}	68	
NF[a] [9]-Chile	0.000 25	0.021	6	16	7.6×10^{11}	70	16.9
	0.000 1	0.08	4.5	3	5.5×10^{9}	32[a]	0.65[a]

[a] Some very small devices, recently developed, are probably not optimized yet. The energy density parameter has a value of the order of (1–10) $\times 10^{10}$ J m^{-3} for all the experimentally optimized machines listed. The drive parameter has practically the same value for all the experimentally optimized machines listed (68–95 kA cm^{-1} mbar$^{-1/2}$). A new parameter related to the energy per mass was introduced now, 'energy per mass parameter' E/a^3p. Note that the three parameters listed in the right-hand side columns are practically constant in comparison throughout the eight orders of magnitude in stored energy range.

is of the order of $\pi(0.12a^2) \times (0.8a) = 0.036a^3$, and the plasma energy density at the pinch moment is proportional to $E/V_p \sim 28E/a^3$. Soto observed that the value of this parameter, $28E/a^3$, is roughly constant in various devices that operate at different energies.

The constancy of these parameters for any PF experimentally optimized for neutron emission and the fact that the dimensions of the pinch, length z_p and radius r_p, are both proportional to the anode radius a have interesting consequences.

(a) The magnetic field at the pinch radius has practically the same value for PF devices with energies from 1 MJ to less than 1 J. This statement is a consequence of the variation of nearly one order of magnitude in the operating pressure and the constancy of the drive parameter. The mass per unit volume p (or pressure) ranges on order of magnitude, thus $p^{1/2}$ varies by nearly 30%. As the magnetic field is proportional to $I_0/r_p \propto I_0/a$ and the drive parameter remains constant in devices operating in a wide range of energies, it is possible to roughly consider that I/a could vary only in the order of 30% in the same range of devices with different energies. Therefore it is possible to obtain at the edge of the pinch magnetic fields of the order of 30 to 40 T, in any of the PF with initial stored energy of MJ, kJ, J or less than 1 J.

(b) The ion pinch density is proportional to the filling gas density (or filling mass, or filling pressure). To estimate the average ion density in the pinch, $\langle n \rangle$, in PF devices, we consider the sweep gas onto the anode from the filling gas density, n_0, compressed to the pinch radius, r_p, thus $\langle n \rangle = f_{mr} n_0 (a/r_p)^2$, with f_{mr} the ionization mass factor in the radial phase and n_0 the number of atoms per volume at filling pressure. Considering that $r_p \sim 0.12a$ and $f_{mr} \sim 0.25$ (typical values from numerical simulations [30] and also experimentally measured [5, 19]), an average pinch ion density of the order of $\langle n \rangle = 18n_0$ is estimated. Typically the filling gas pressure is of a few mbars. Thus the value of $\langle n \rangle = 18n_0$ is consistent with the n value measured experimentally on the pinch axis of the order of 10^{25} m^{-3}, i.e. an average of the order of 5×10^{24} m^{-3} for a PF with initial stored energy of MJ, kJ, J or less than 1 J, in any of them.

(c) The mean Alfvén speed is practically the same for any PF experimentally optimized for neutron emission. The mean Alfvén speed for a Z-pinch is $\langle v_{alfven} \rangle = B(r = r_p)/2(\mu_0 \langle r_p \rangle)^{1/2}$, with $\langle \rho_p \rangle$ the mean pinch mass density. Following the arguments presented in (b) it is clear that $\langle \rho_p \rangle$ is proportional to the filling gas density or filling gas pressure. Thus, $\langle v_{alfven} \rangle \propto I_0/ap^{1/2}$, and its value can be estimated to be above 10^5 m s^{-1}.

(d) The temperature in the pinch is of the same order of magnitude in any PF experimentally optimized for neutron emission. This statement is valid for the two main mechanisms that contribute to the heating of the plasma in a PF: the shock wave in the radial phase and the current at the pinch moment. On the one hand, for a strong shock system, approximately 50% of the shock kinetic energy is converted into the thermal energy in the shock layer. As it has been established that kinetic energy per unit mass of

the plasma sheath is proportional to $I^2/a^2 p$ [31], it means that the square of the drive parameter is a measure of the energy per unit mass.

On the other hand, the contribution to heating by the current can be estimated by the Bennett relation:

$$kT_B = (\mu_0/16\pi)I^2/N,$$

with N the number of ions per unit length (ion line density),

$$N = 2\pi \int nr\,\mathrm{d}r,$$

$$\langle n\rangle = N/\pi r_p^2,$$

$$N = \langle n\rangle \pi r_p^2 \propto n_0 a^2,$$

$$kT_B \propto I^2/n_0 a^2 \propto I^2/a^2 p.$$

Therefore, the Bennett temperature is proportional to the square value of the drive parameter.

As the two main heating mechanisms are proportional to the square value of the drive parameter, it is possible to conclude that the plasma temperature in the pinch does not deviate much among different devices with energies from megajoules to less than 1 J.

The statement can also be analyzed using other constant parameters (the energy density parameter E/V_p and the mean ion density n). Combining these parameters, the quantity $E/(V_p n)$ is also constant. The latter parameter represents the energy per ion, which defines the ion temperature. Thus,

$$T \propto E/(V_p n).$$

Therefore, any PF device with a similar energy density parameter and ion density has a temperature of the same order.

The last column of table 2 includes a parameter proportional to the energy per ion. Note that for devices with stored energy ranging eight orders of magnitude, the energy per particle parameter (essentially the energy per mass parameter, $E/a^3 p$) ranges in the same order of magnitude for neutron optimized PF (only a factor 1/23 versus a factor $1/10^8$).

As previously discussed, on eight orders of magnitude of variation in stored energy, the drive parameter varies only by a factor of 2 while the energy density parameter varies by a factor of 10 and the energy per mass parameter varies by a factor of 23. The energy density and energy per mass parameters are essentially proportional to the square of drive parameter, thus only a variation by a factor of 4 should be expected. However, it is necessary to remember that for calculating the energy density parameter, $E/V_p \sim 28E/a^3$, and the energy per mass parameter, $E/a^3 p$, the pinch radius is considered to be $0.15a$, but actually the pinch radius could vary from $0.1a$ to $0.2a$. Therefore, a variation factor of $2^3 = 8$ in the energy density parameter is possible. In the case of the energy per mass parameter, the variation in the filling pressure could also be considered which would increase the expected variation of this parameter. In spite of these considerations, a variation by a factor of 10 or 23 compared with a factor of 10^8 could be considered negligible. However, it can be clearly seen in table 2 that the most constant parameter is the 'drive parameter'.

3.2. Differences

Even though several plasma parameters remain practically with the same value in any PF experimentally optimized for neutron emission, there is an important difference which determines the stability properties of the plasma pinch. As the ion pinch density, n, is practically the same, but the pinch radius changes, the line density N is different in every device and depends on the stored energy and on the anode radius.

$$N \propto a^2 n,$$

$$E/V_p n = \text{const.} \rightarrow E \propto V_p n \propto a^3 n.$$

Thus, $N \propto E/a$.

As the stability properties in a Z-pinch depend on the line density N and other parameters, it means that the stability regime, in which a particular PF device lives, depends on the energy of the device and on the anode radius.

It is well known that a large majority of the modern Z-pinch experiments operate in a region of parameter space in which ideal MHD stability is not applicable. The stability behavior can be discussed in terms of certain dimensionless parameters. This can be visualized in the diagram for regimes of Z-pinch stability developed by Haines and Coppins [32]. If the Bennett equilibrium holds, the stability can be characterized in terms of the line density N and the product between the total pinch current raised to the fourth power and the pinch radius $I^4 r_p$. Details of this diagram can be found elsewhere [32]. In particular for a Z-pinch in deuterium the Lundquist number S, the product between the ion Larmor Ω_i and the ion collision frequency τ_i and the mean ion Larmor radius a_i can be written as

$$S = 3.86 \times 10^{23} I^4 r_p/N,$$

$$\Omega_i \tau_i = 3.64 \times 10^{30} I^4 r_p/N^{5/2},$$

$$a_i/r_p = 8.08 \times 10^{30} N^{-1/2}.$$

It has been theoretically conjectured that there is a threshold for stabilization due to resistive effects corresponding to $S \sim 100$; enhanced stability is expected if $S < 100$ [32]. In addition, it has been experimentally observed that for Z-pinches with a value of $S < 100$, no instabilities are observed [35–38]. Also large Larmor radius (LLR) effects play a stabilization role. The LLR stabilization effects are important when $a_i/r_p > 0.1$ and if $\Omega_i \tau_i > 1$.

Most of the theoretical works on this topic use the basic Vlasov fluid model to treat the ions, where it is obtained that the LLR effects can reduce linear growth rates of the instabilities by up to a factor of about 5 for $m = 0$ and 8 for $m = 1$. Theoretically, the lowest growth rate occurs for $a_i/r_p \sim 0.1$–0.2 [33, 34]. There exists experimental evidence indicating that enhanced stability is found for values of a_i/r_p close to 0.1–0.2 for both $m = 1$ [24, 36, 37] and $m = 0$ [39] instabilities.

All the PF devices listed in table 2 are plotted in the diagram for Z-pinch stability regimes (figure 3). Although the pinch current is a fraction of the peak current (typically

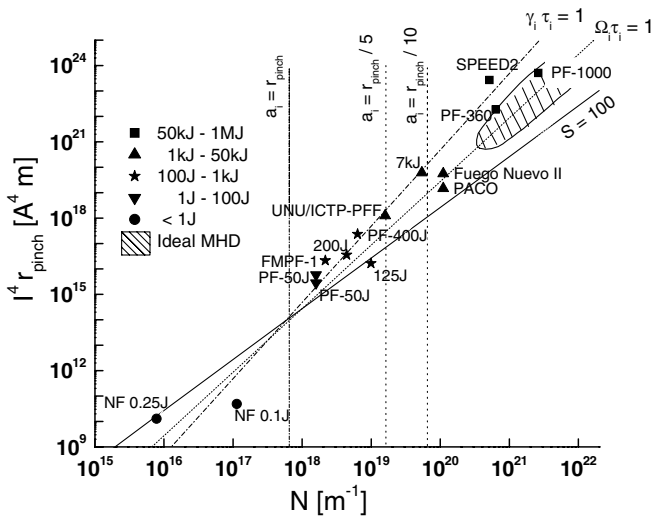

Figure 3. Different plasma foci that work with stored energy ranging from 0.1 J to 1 MJ are plotted in the diagram for Z-pinch stability given by Haines and Coppins [32].

0.8–0.9 from numerical simulations fitted with experimental results [30]) the peak current I_0 of table 2 was used. The log plot and the scale used practically absorb this difference. The line density was estimated for each device using the relation $N = \langle n \rangle \pi r_p^2$, with $r_p = 0.15a$.

From the diagram in figure 3, it is possible to note that large PF devices (hundreds of kilojoules and megajoules) are in the ideal MHD region, and are unstable. In contrast, the smallest device with stored energy less than 1 J, Nanofocus, could be stabilized by means of the resistive effects. With more current, the PF devices in the range of hundreds and tens of joules could be stabilized by means of the LLR effects [24].

4. Conclusions

A comprehensive study of the scaling laws together with similarities and differences in PF devices working with stored energy ranging eight orders of magnitude, from 1 MJ to 0.1 J was presented. From the study it is possible to draw the following conclusions for any PF experimentally optimized for neutron emission, independent of the initial stored energy.

- The pinch radius and pinch length scale with the anode radius, and $r_p \sim (0.1\text{–}0.2)a$, $z_p \sim (0.8\text{–}1)a$ [5, 8, 17, 19, 30].
- The mean value of the pinch ion density scales with the filling gas density, and $\langle n \rangle \sim 18 n_0 \sim 5 \times 10^{24}$ m^{-3}.
- The drive parameter, the energy density parameter and the energy per mass parameter have practically the same value for any PF experimentally optimized for neutron emission. This implies the following:
- The magnetic field at the pinch edge has a value of the order of 30–40 T for any PF experimentally optimized for neutron emission.
- The Alfvén speed in the pinch has practically the same value in any PF experimentally optimized for neutron emission.
- Any PF device with a similar drive parameter, energy density parameter and ion density has a temperature of the same order. Thus, an experimental measurement of temperature in a particular PF could be used to estimate the temperature of any PF experimentally optimized for neutron emission. In [40] the temperature was measured in a PF of some kilojoules by means of spectroscopy techniques as ∼0.6–1 keV. Then, it is possible to assume that the temperature in any PF operating properly, including the smallest ones such as the PF-50J and the Nanofocus, has a temperature of that order.

The PF is a self-scaled device. However, the stability regime, in which a particular PF device lives, depends on the energy of the device and the anode radius. Large PF devices (hundreds of kilojoules and megajoules) are in the ideal MHD region, and are unstable. In contrast, the smallest device with stored energy less than 1 J, Nanofocus, could present enhanced stability by means of the resistive effects. PF devices in the range of hundreds and tens of joules could present enhanced stability by means of LLR effects.

An open challenge for PF research, for both basic and applied science, is to increase the energy per particle (temperature) in order to increase the neutron yield. Is there any operational region in which this could be possible? The PF is a self-scaled device; however, the dependence of the stability properties on the energy of the device and on the anode radius could open this possibility.

Acknowledgments

Currently, this work is supported by the grant P^4 Project 'Center for Research and Applications in Plasma Physics and Pulsed Power Technology', PBCT-CONICYT Chile ACT 26 grant and a Postdoctoral PBCT-CONICYT Chile PSD-01 grant. Also, part of this work was supported by IAEA-CRP contract No. 14722.

References

[1] Serban A and Lee S 1998 *J. Plasma Phys.* **60** 3
[2] Soto L 2005 *Plasma Phys. Control. Fusion* **47** A361
[3] Soto L, Esaulov A, Moreno J, Silva P, Sylvester G, Zambra M, Nazarenko A and Clausse A 2001 *Phys. Plasmas* **8** 2572
[4] Silva P, Soto L, Moreno J, Sylvester G, Zambra M, Altamirano L, Bruzzone H, Clausse A and Moreno C 2002 *Rev. Sci. Instrum.* **73** 2583
[5] Moreno J, Silva P and Soto L 2003 *Plasma Sources Sci. Technol.* **12** 39
[6] Silva P, Moreno J, Soto L, Birstein L, Mayer R and Kies W 2003 *Appl. Phys. Lett.* **83** 3269
[7] Silva P, Soto L, Kies W and Moreno J 2004 *Plasma Sources Sci. Technol.* **13** 329
[8] Soto L, Silva P, Moreno J, Zambra M, Kies W, Mayer R E, Clausse A, Altamirano L, Pavez C and Huerta L 2008 *J. Phys. D: Appl. Phys.* **41** 205215
[9] Soto L, Pavez C and Moreno J, Barbaglia M and Clausse A 2009 *Plasma Sources Sci. Technol.* **18** 015007
[10] Milanese M, Moroso R and Pouzo J 2003 *Eur. Phys. J.* D **27** 77
[11] Rout R K, Mishra P, Rawool A M, Kulkarani L V and Gupta S C 2008 *J. Phys. D: Appl. Phys.* **41** 205211

[12] Verma R, Rawat R S, Lee P, Krishnan M, Sprinham S V and Tan T L 2009 *Plasma Phys. Control. Fusion* **51** 075008
[13] Filipov N V, Filipova T I and Vinogradov V P 1962 *Nucl. Fusion* (Suppl.) **2** 577
[14] Mather J W 1964 *Phys. Fluids* (Suppl.) **7** 28
[15] Pouzo J and Milanese M 2003 *IEEE Trans. Plasma Sci.* **31** 1237
[16] Castillo F, Herrera J J E, Rangel J, Milanese M, Moroso R, Pouzo J, Golzarri J I and Espinosa G 2003 *Plasma Phys. Control. Fusion* **45** 289
[17] Lee S and Serban A 1996 *IEEE Trans. Plasma Sci.* **24** 1101
[18] Moreno J, Birstein L, Mayer R E, Silva P and Soto L 2008 *Meas. Sci. Technol.* **19** 087002
[19] Tarifeño A, Pavez C, Moreno J and Soto L 2009 Dynamics and density measurements in a small plasma focus of tens of joules emitting neutrons, submitted
[20] Kies W 2002 private communication
[21] Pavez C, Moreno J, Silva P, Castillo F, Herrera J and Soto L 2008 *J. Phys.: Conf. Ser.* **134** 012049
[22] Da Re A, Mezzetti F, Tartari A, Verri G, Rapezzi L and Gribkov V A 2001 *Nukleonika* **46** S123–5
[23] Pavez C and Soto L 2010 *IEEE Trans. Plasma Sci.* **38** 1132
[24] Pavez C and Soto L 2008 *Phys. Scr.* **T131** 014030
[25] Schdmidt H, Kasperczuk A, Paduch M, Pisarczyk T, Scholz M, Tomaszewski K and Szydlowsky A 2002 *Phys. Scr.* **66** 168
[26] Zebrowski J, Baranowski J, Jakubowski L and Sadowski M 2001 *Nukleonika* **46** S1
Zebrowski J, Baranowski J, Jakubowski L and Sadowski M 2001 *Nukleonika* **46** S65
[27] Kashani M A M and Miyamoto T 2002 Dense Z-pinches *5th Int. Conf. on Dense Z-Pinch (Albuquerque, NM, 2001) AIP Conf. Proc.* **651** 249
[28] Moreno C, Bruzzone H, Martinez J and Clausse A 2000 *IEEE Trans. Plasma Sci.* **28** 1735
[29] Lee S *et al* 1988 *Am. J. Phys.* **56** 62
[30] Lee S *Radiative Dense Plasma Focus Computation Package: RADPF* http://www.intimal.edu.my/school/fas/UFLF/; http://www.plasmafocus.net/IPFS/modelpackage/File1RADPF.htm
[31] Zhang T, Rawat R S, Hassan S M, Lin J J, Mahmood S, Tan T L, Springham S V, Gribkov V A, Lee P and Lee S 2006 *IEEE Trans. Plasma Sci.* **34** 2356
[32] Haines M G and Coppins M 1991 *Phys. Rev. Lett.* **66** 1462
[33] Arber T D, Coppins M and Scheaffel J 1994 *Phys. Rev. Lett.* **72** 2399
[34] Arber T D *et al* 1995 *Phys. Rev. Lett.* **74** 2698
[35] Chuaqui H, Soto L, Favre M and Wyndham E 1994 *Proc. 3rd Int. Conf. on Dense Z-Pinches (London, UK, 1993) AIP Conf. Proc.* **299** 27
[36] Soto L, Chuaqui H, Favre M and Wyndham E 1994 *Phys. Rev. Lett.* **72** 2891
[37] Soto L, Chuaqui H, Favre M, Saavedra R, Wyndham E, Skowronek M, Romeas P, Aliaga-Rossel R and Mitchell I 1998 *IEEE Trans. Plasma Sci.* **24** 1162
[38] Soto L, Chuaqui H, Favre M and Wyndham E 1994 *Proc. Int. Conf. on Plasma Physics ICPP 1994 (Foz do Iguazú, Brazil)* p 216
[39] Davies H, Dangor A, Coppins M and Haines M 2001 *Phys. Rev. Lett.* **87** 145004
[40] Bergmann K, Rosmej O N, Rosmej F B, Engel A, Gavrilescu C, Neff W and Lebert R 1997 *Phys. Rev.* E **56** 5959
[41] Decker G, Kies W, Mälzig M, Van Valker C and Ziethen G 1986 *Nucl. Instrum. Methods* A **249** 477
[42] Pouzo J and Milanese M 2007 *Proc. 4th Symp. on Current Trends in International Fusion Research (Washington, DC, 2001)* (Ottawa: NRC Research Press) NRC 46856 p 33
[43] Zakaullah M, K Alamgir, Shafiq M, Hassan S M, Sharif M and Waheed A 2001 *Appl. Phys. Lett.* **78** 877
[44] Lee S, Saw S H, Lee P and Rawat R S 2009 *Plasma Phys. Control. Fusion* **51** 105013
[45] Rapp H 1973 *Phys. Lett.* A **43** 420
[46] Kromholz H, Ruhl F, Schneider W, Schonbach K and Herziger G 1981 *Phys. Lett.* A **82** 82
[47] Bernard A *et al* 1998 *J. Moscow Phys. Soc.* **8** 93
[48] Lee S and Saw S H 2008 *J. Fusion Energy* **27** 292
[49] Lee S 2008 *Plasma Phys. Control. Fusion* **50** 105005
[50] Lee S 2009 *Appl. Phys. Lett.* **95** 151503